Chapter 11: Regional Climate Projections
Figures

Coordinating Lead Authors: Jens Hesselbjerg Christensen (Denmark), Bruce Hewitson (South Africa)

Lead Authors: Aristita Busuioc (Romania), Anthony Chen (Jamaica), Xuejie Gao (China), Isaac Held (USA), Richard Jones (UK), Won-Tae Kwon (Korea), René Laprise (Canada), Victor Magaña Rueda (Mexico), Linda Mearns (USA), Claudio Guillermo Menéndez (Argentina), Jouni Räisänen (Finland), Annette Rinke (Germany), Rupa Kumar Kolli (India), Abdoulaye Sarr (Senegal), Penny Whetton (Australia)

Contributing Authors: *Raymond Arritt (USA),* Rasmus Benestad (Norway), Martin Beniston (Switzerland), David Bromwich (USA), Daniel Caya (Canada), Josefino Comiso (USA), Ramón de Elía (Canada, Argentina), Klaus Dethloff (Germany), Seita Emori (Japan), Johannes Feddema (USA), Rüdiger Gerdes (Germany), Jesus Fidel Gonzales-Rouco (Spain), William Gutowski (USA), Inger Hanssen-Bauer (Norway), Colin Jones (Canada), Robert Katz (USA), Akio Kitoh (Japan), Reto Knutti (USA, Switzerland), Ruby Leung (USA), Jason Lowe (UK), Amanda H. Lynch (Australia), Christoph Matulla (Germany), Kathleen McInnes (Australia), Anna V. Mescherskaya (Russia), Brett Mullan (New Zealand), Mark New (UK), Majid Habibi Nokhandan (Iran), Jeremy S. Pal (Italy), David Plummer (Canada), Markku Rummukainen (Sweden, Finland), Christoph Schär (Switzerland), Samuel Somot (France), Daíthí A. Stone (UK), Ramasamy Suppiah (Australia), Mark Tadross (South Africa), Claudia Tebaldi (USA), Warren Tennant (South Africa), Martin Widman (Germany, UK), Rob Wilby (UK), Bruce L. Wyman (USA)

Review Editors: Congbin Fu (China), Filippo Giorgi (Italy)

Date of Draft: 27 October 2006

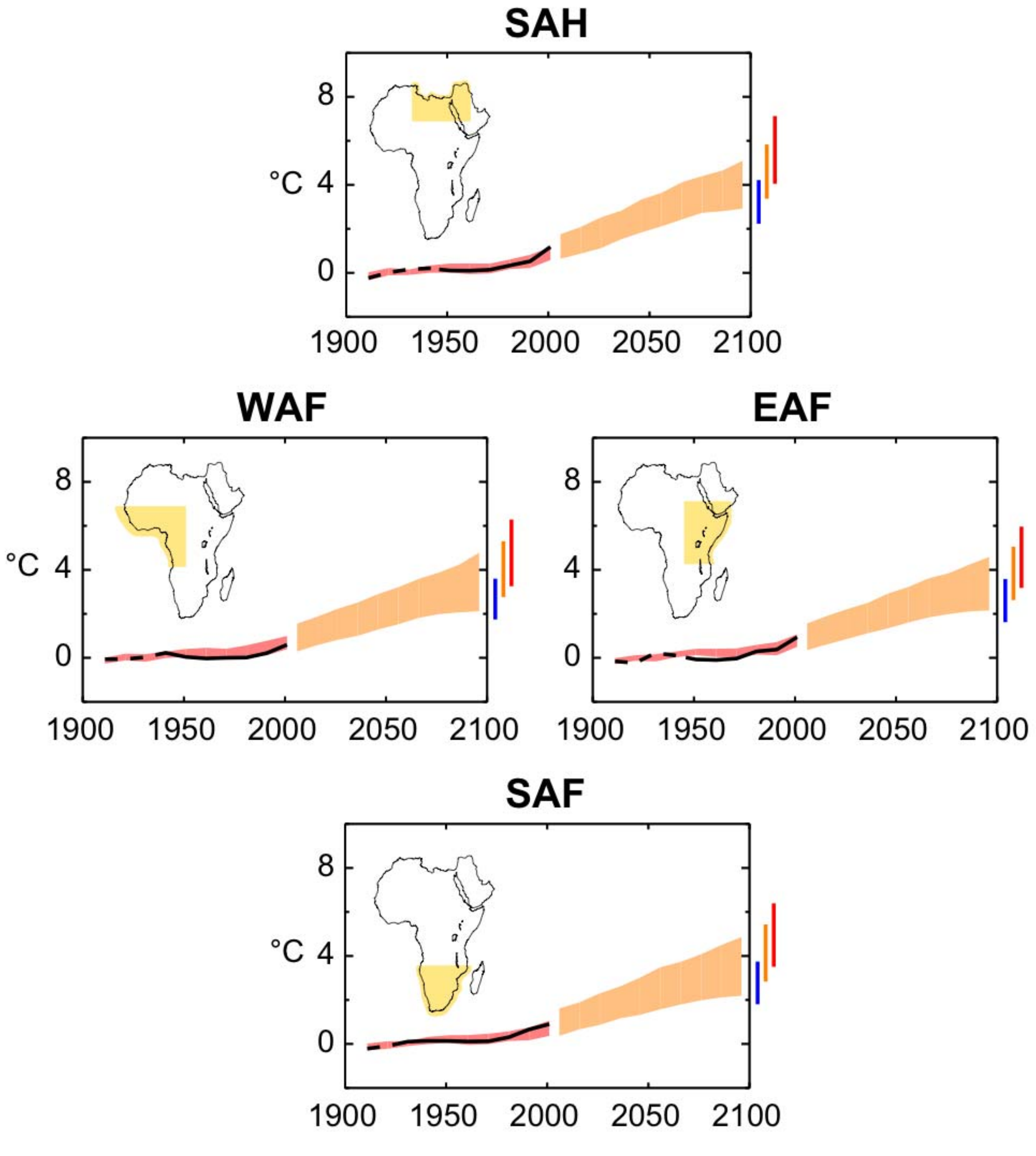

Figure 11.1. Temperature anomalies with respect to 1901–1950 for four African land regions for 1906–2005 (black line) and as simulated (red envelope) by MMD models incorporating known forcings; and as projected for 2001–2100 by MMD models for the A1B scenario (yellow envelope). The bars at the end of the yellow envelope represent the range of projected changes for 2091–2100 for the B1 scenario (blue), the A1B scenario (yellow) and the A2 scenario (red). The black line is dashed where observations are present for less than 50% of the area in the decade concerned. More details on the construction of these figures is given in Box 11.1 and Section 11.1.2

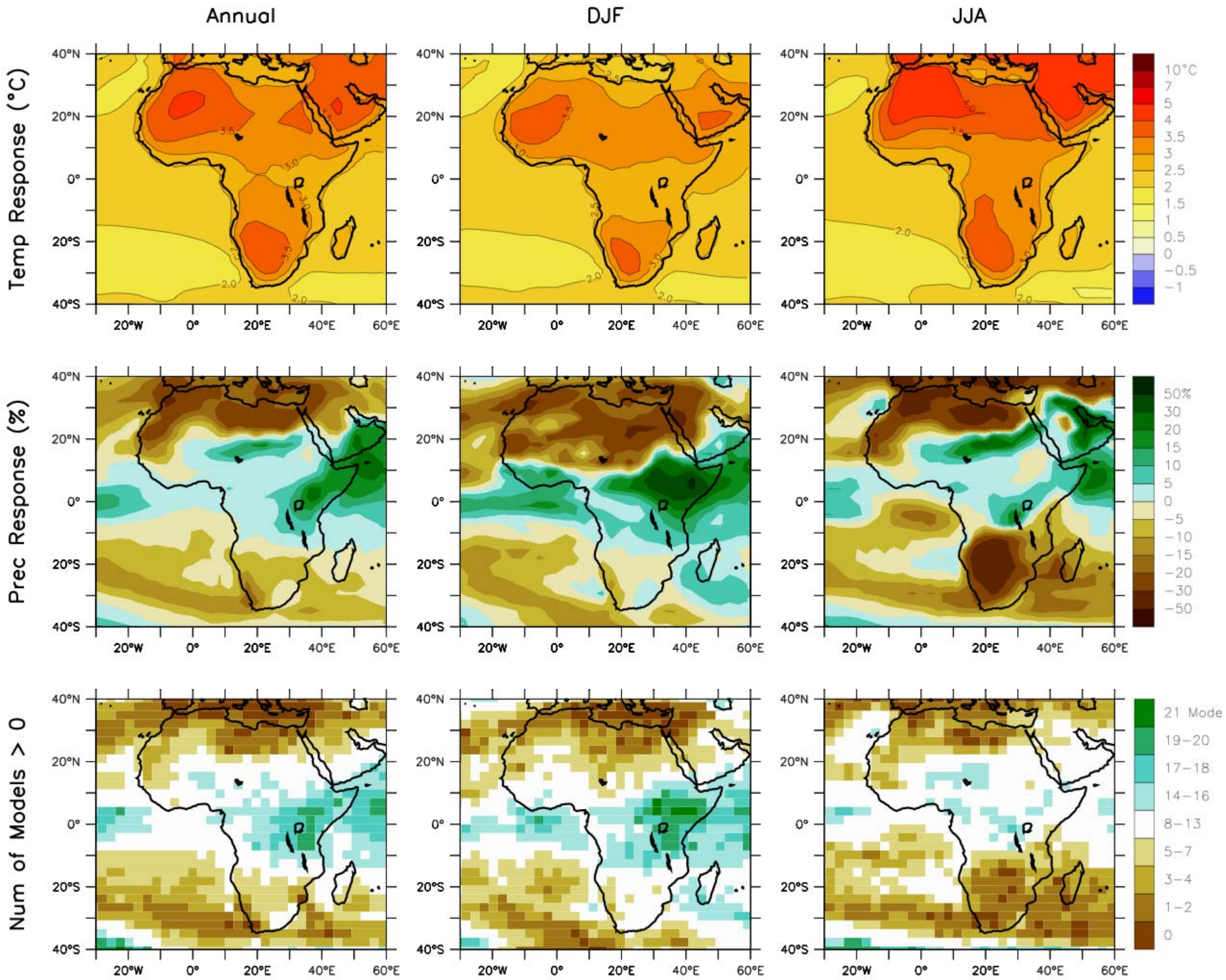

Figure 11.2. MMD-A1B temperature and precipitation changes over Africa. Top row: Annual mean, December-January-February, and June-July-August temperature change between 1980–1999 and 2080–2099, averaged over 21 models. Middle row: same for fractional change in precipitation. Bottom row: number of models out of 21 that project precipitation to increase.

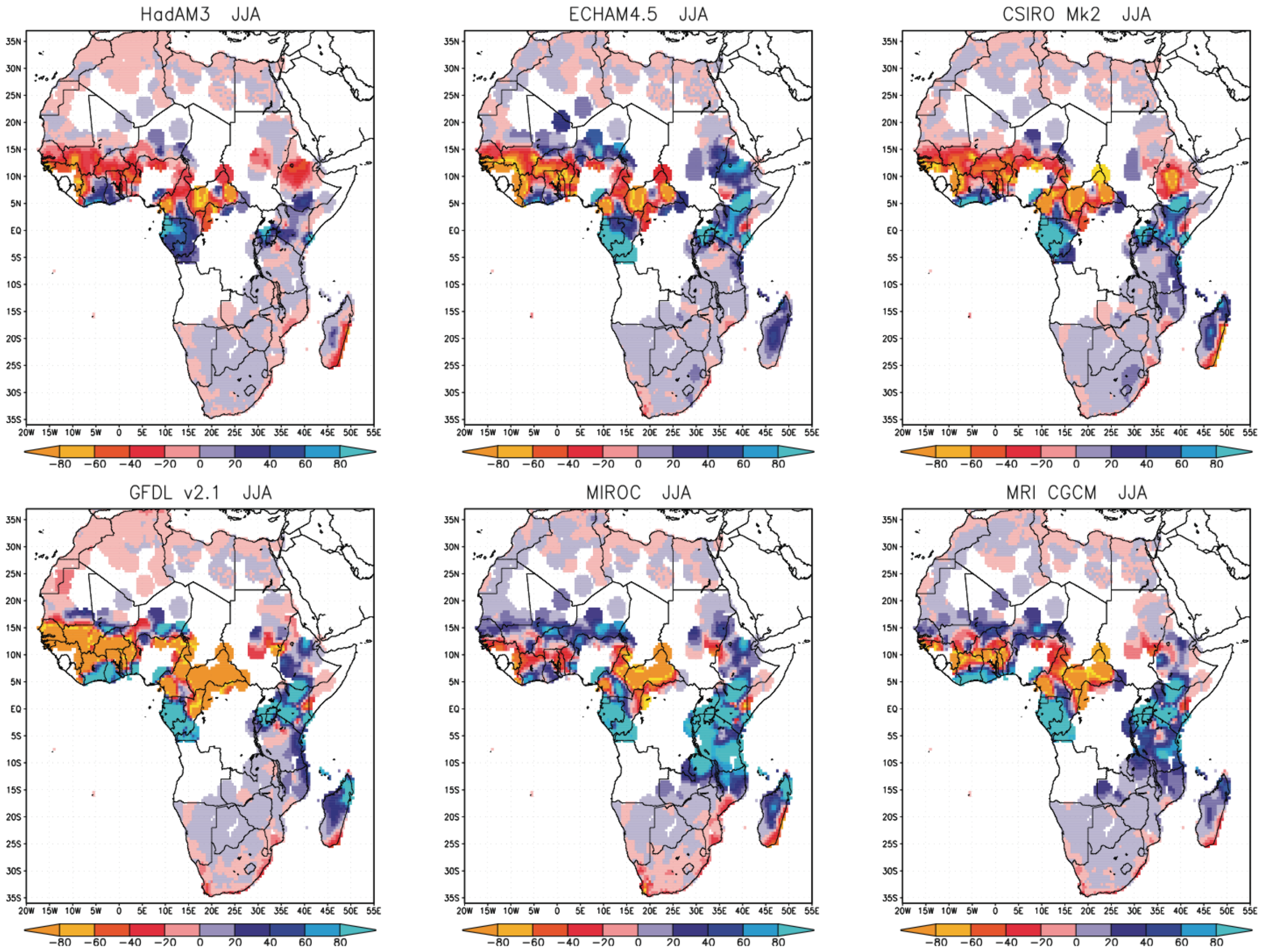

Figure 11.3. Anomaly of mean monthly precipitation (mm) daily data empirically downscaled from 6 GCMs (ECHAM4.5, HadAM3, CSIRO Mk2, GFDL 2.1, MRI, MIROC) to 858 station locations. GCMs are forced by the SRES A2 scenario. Anomalies are for the future period (2070–2099 for the first three models, and 2080–2099 for the latter three models) minus a control 30 year period (from Hewitson and Crane, 2006).

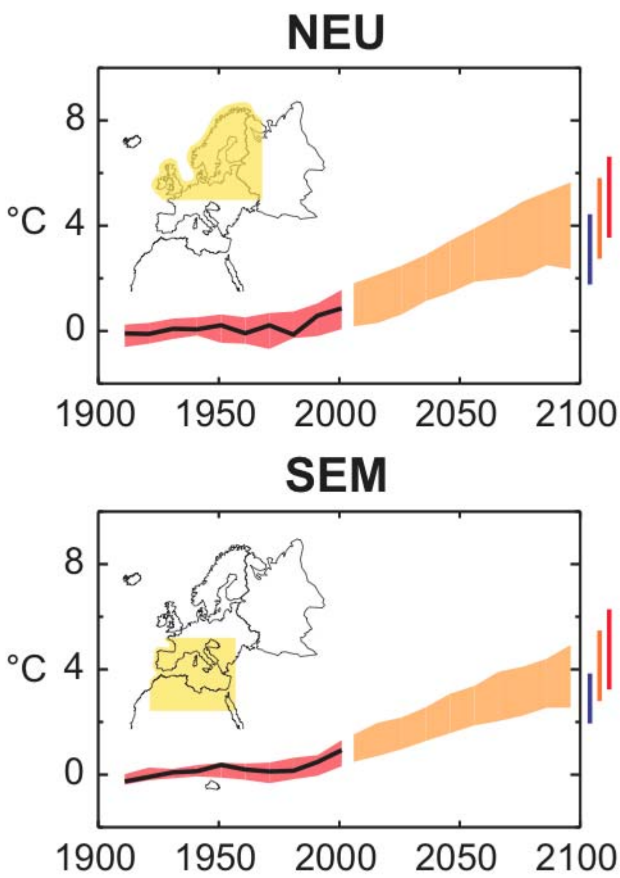

Figure 11.4. Temperature anomalies with respect to 1901–1950 for two Europe land regions for 1906–2005 (black line) and as simulated (red envelope) by MMD models incorporating known forcings; and as projected for 2001–2100 by MMD models for the A1B scenario (yellow envelope). The bars at the end of the yellow envelope represent the range of projected changes for 2091–2100 for the B1 scenario (blue), the A1B scenario (yellow) and the A2 scenario (red). The black line is dashed where observations are present for less than 50% of the area in the decade concerned. More details on the construction of these figures is given in Box 11.1 and Section 11.1.2

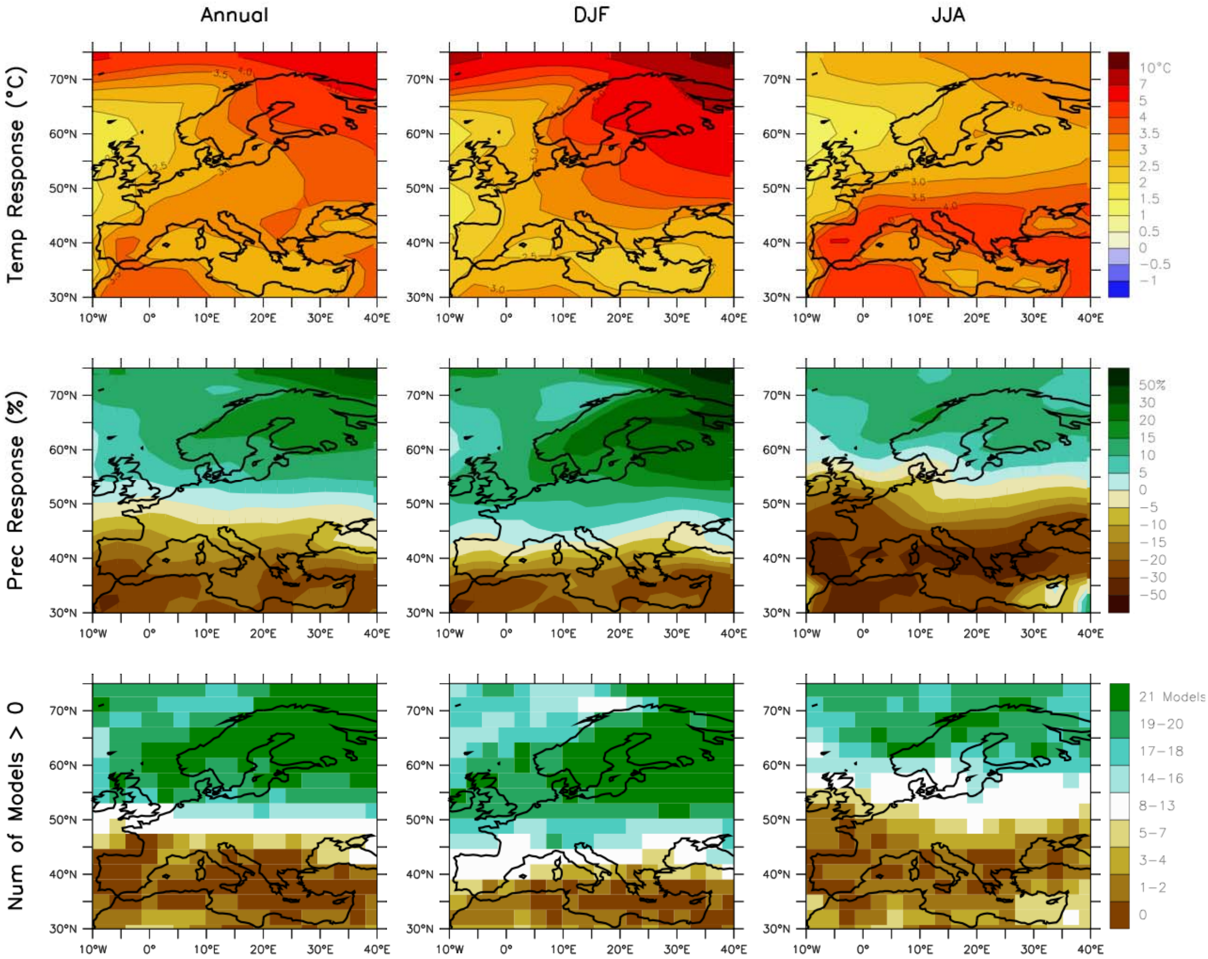

Figure 11.5. MMD-A1B temperature and precipitation changes over Europe. Top row: Annual mean, December-January-February, and June-July-August temperature change between 1980–1999 and 2080–2099, averaged over 21 models. Middle row: same for fractional change in precipitation. Bottom row: number of models out of 21 that project precipitation to increase.

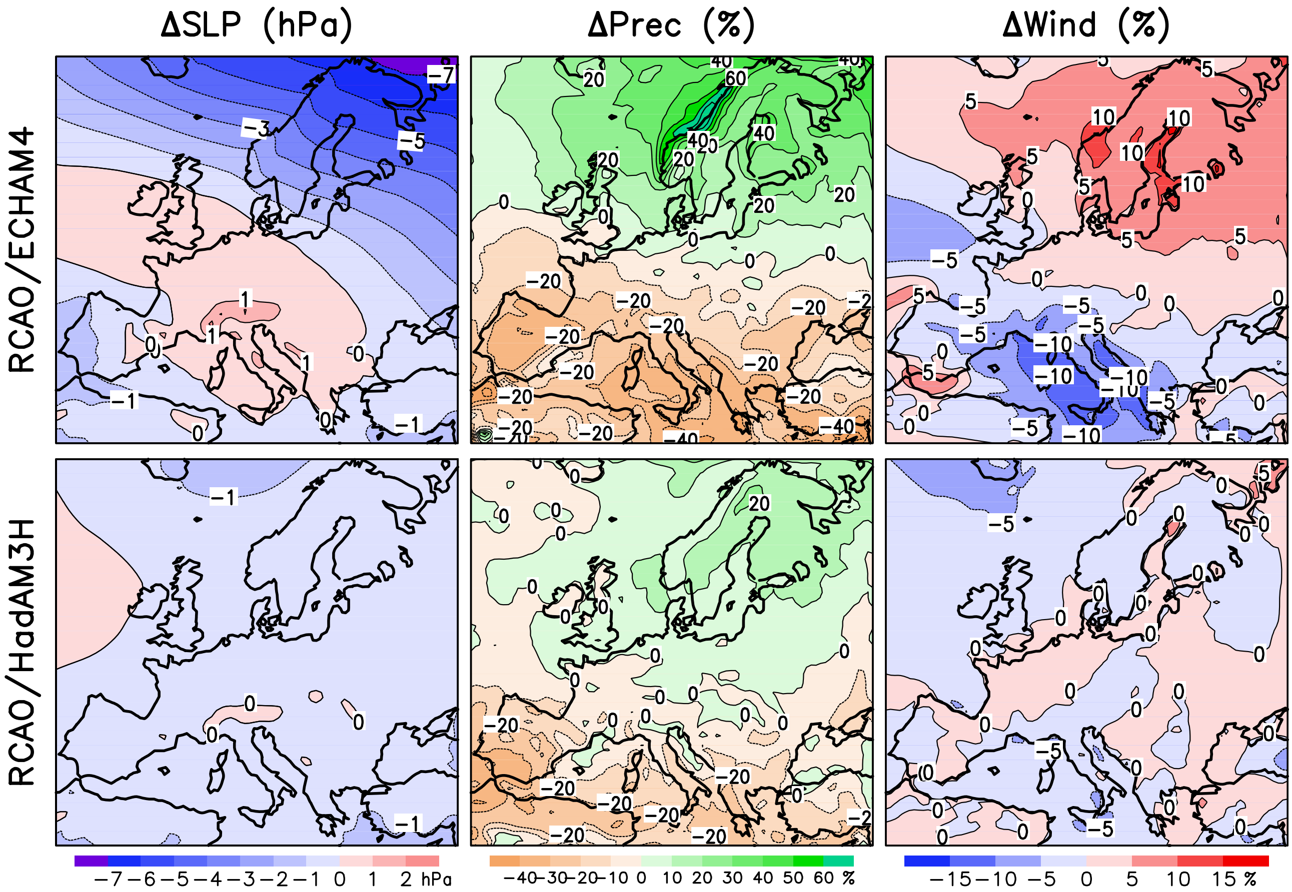

Figure 11.6. Simulated changes in annual mean sea level pressure (ΔSLP), precipitation (ΔPrec) and mean 10 m level wind speed (ΔWind) from the years 1961–1990 to the years 2071–2100. The results are based on the SRES A2 scenario and were produced by the same RCM (RCAO) using boundary data from two global models: ECHAM4/OPYC3 (top) and HadAM3H (bottom) (redrawn from Rummukainen et al., 2004).

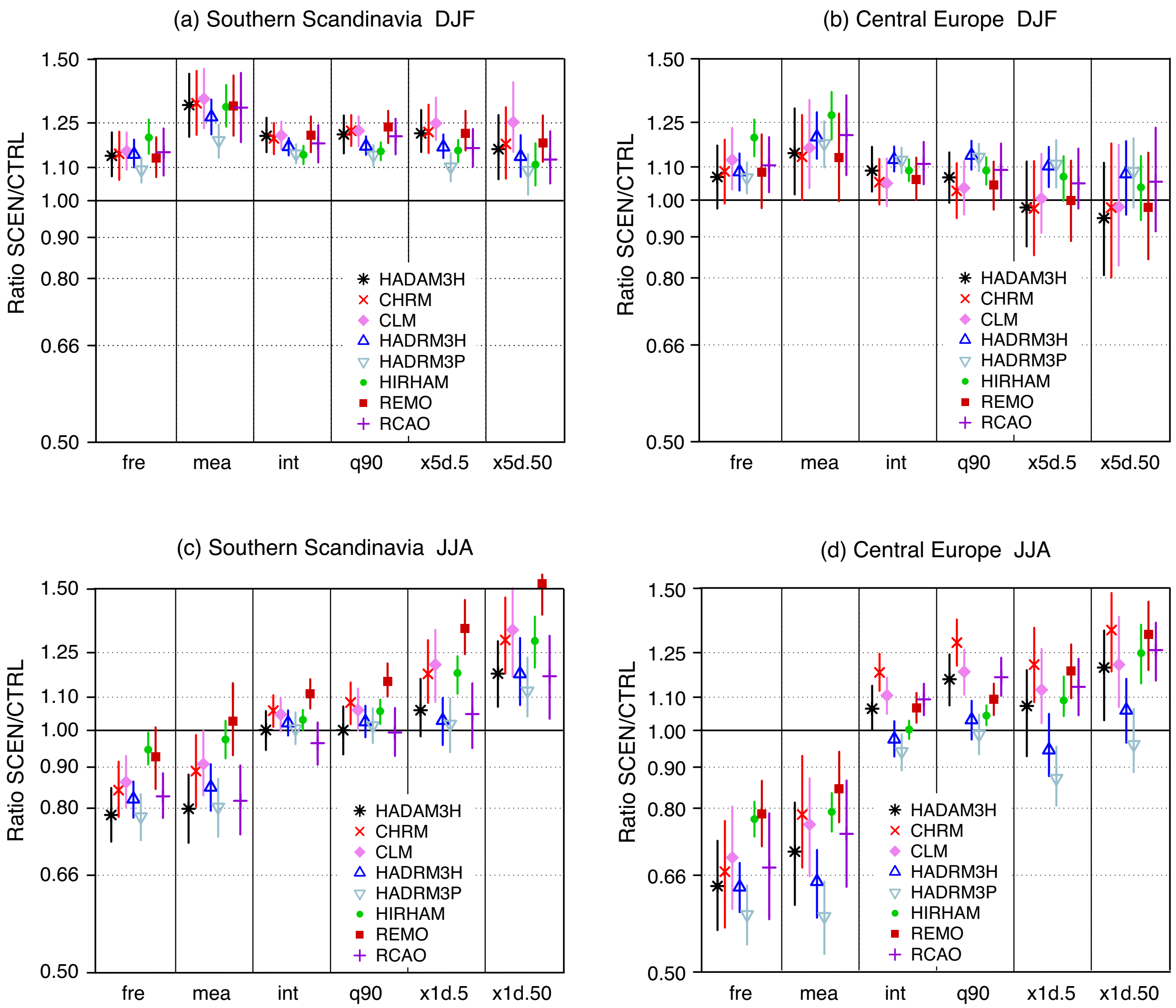

Figure 11.7. Changes (ratio 2071–2100/1961–1990 for the A2 scenario) in domain-mean precipitation diagnostics in the PRUDENCE simulations in southern Scandinavia (5–20°E, 55–62°N) and central Europe (5–15°E, 48–54°N) in winter (top) and in summer (bottom). *fre* = wet-day frequency; *mea* = mean seasonal precipitation; *int* = mean wet-day precipitation; *q90* = 90th percentile of wet-day precipitation; *x1d.5* and *x1d.50* = 5- and 50-year return values of one-day precipitation; *x5d.5* and *x5d.50* = 5- and 50-year return values of five-day precipitation. For each of the eight models, the vertical bar gives the 95% confidence interval associated with sampling uncertainty (redrawn from Frei et al., 2006).

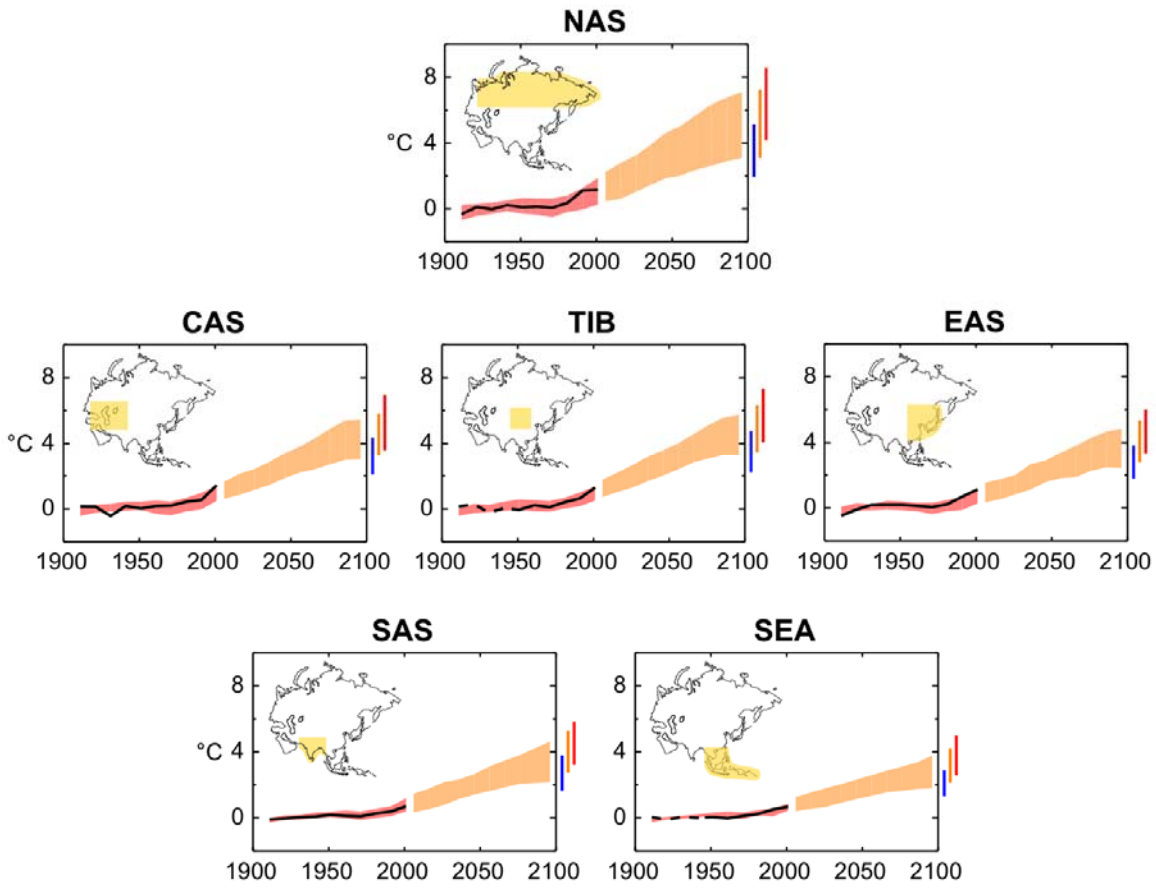

Figure 11.8. Temperature anomalies with respect to 1901-1950 for six Asian land regions for 1906–2005 (black line) and as simulated (red envelope) by MMD models incorporating known forcings; and as projected for 2001–2100 by MMD models for the A1B scenario (yellow envelope). The bars at the end of the yellow envelope represent the range of projected changes for 2091-2100 for the B1 scenario (blue), the A1B scenario (yellow) and the A2 scenario (red). The black line is dashed where observations are present for less than 50% of the area in the decade concerned. More details on the construction of these figures is given in Box 11.1 and Section 11.1.2

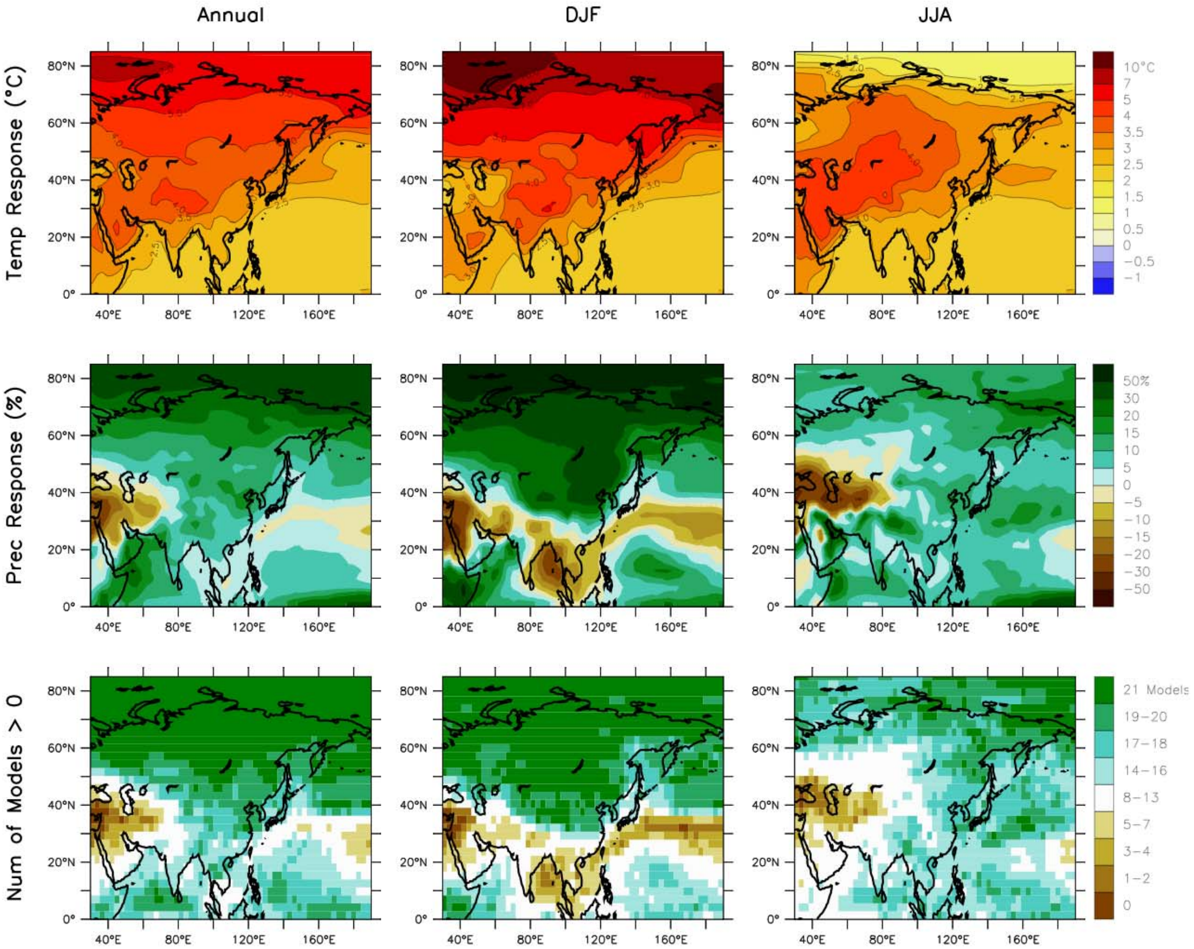

Figure 11.9. MMD-A1B temperature and precipitation changes over Asia. Top row: Annual mean, December-January-February, and June-July-August temperature change between 1980–1999 and 2080–2099, averaged over 21 models. Middle row: same for fractional change in precipitation. Bottom row: number of models out of 21 that project precipitation to increase.

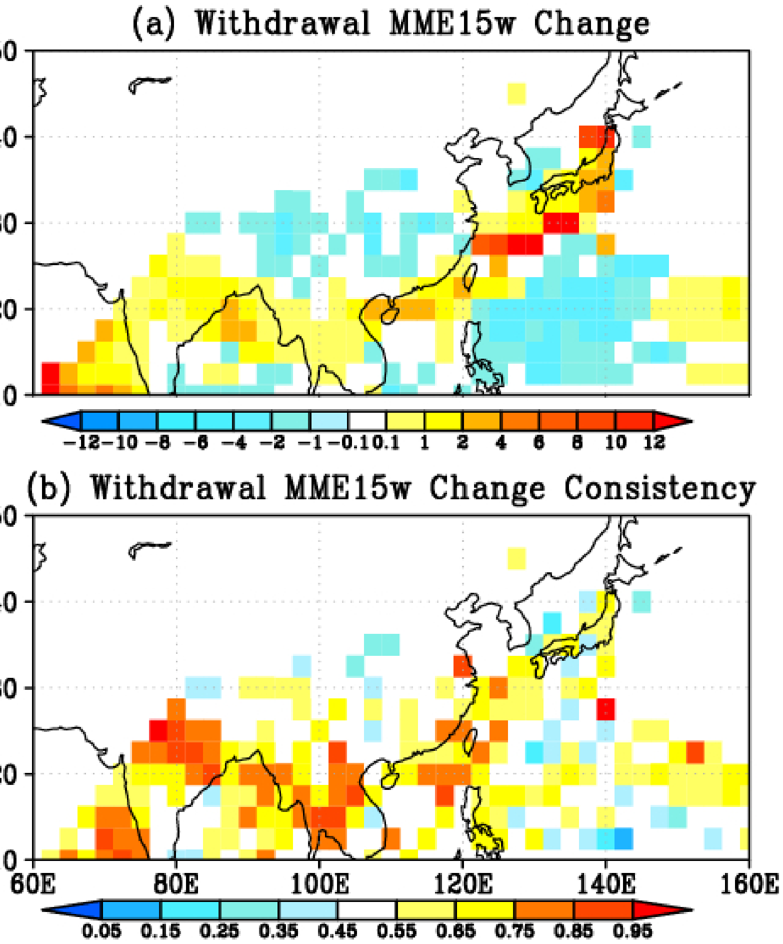

Figure 11.10. (a) Changes in withdrawal dates (pentad) of the Asian summer rainy season based on the 15 AOGCM ensemble climatological pentad mean precipitation between the 2081–2100 of the SRES A1B experiments and the present day (1981–2000) of the 20C3M experiments. (b) Fraction of model numbers with positive difference of onset dates from the present to the future. (Kitoh and Uchiyama, 2006)

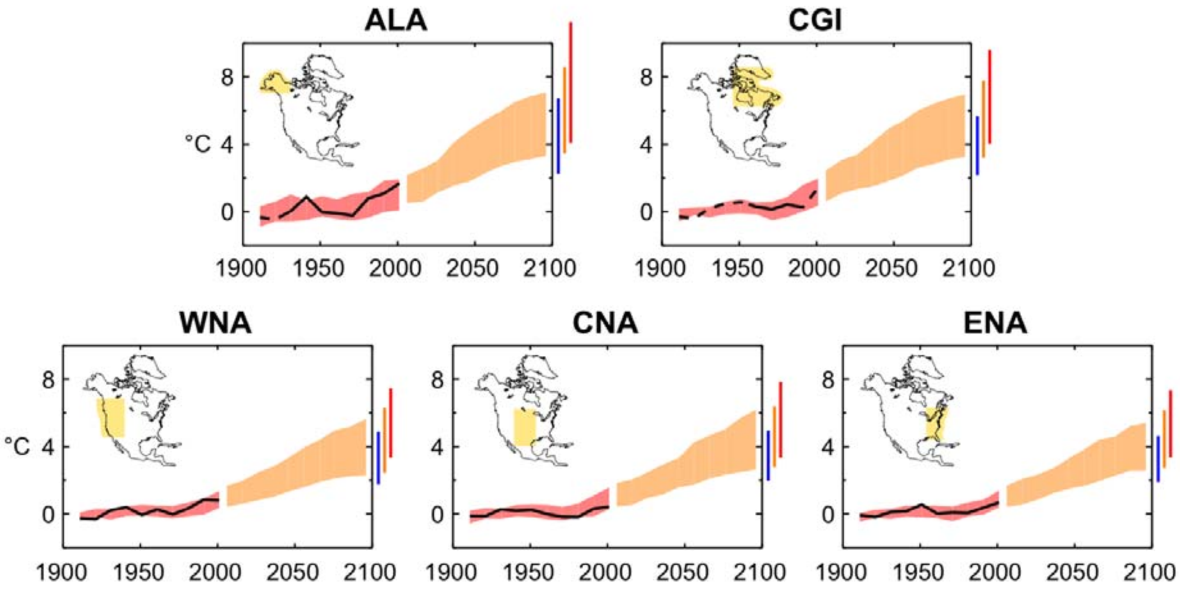

Figure 11.11. Temperature anomalies with respect to 1901–1950 for five North American land regions for 1906–2005 (black line) and as simulated (red envelope) by MMD models incorporating known forcings; and as projected for 2001–2100 by MMD models for the A1B scenario (yellow envelope). The bars at the end of the yellow envelope represent the range of projected changes for 2091–2100 for the B1 scenario (blue), the A1B scenario (yellow) and the A2 scenario (red). The black line is dashed where observations are present for less than 50% of the area in the decade concerned. More details on the construction of these figures is given in Box 11.1 and Section 11.1.2

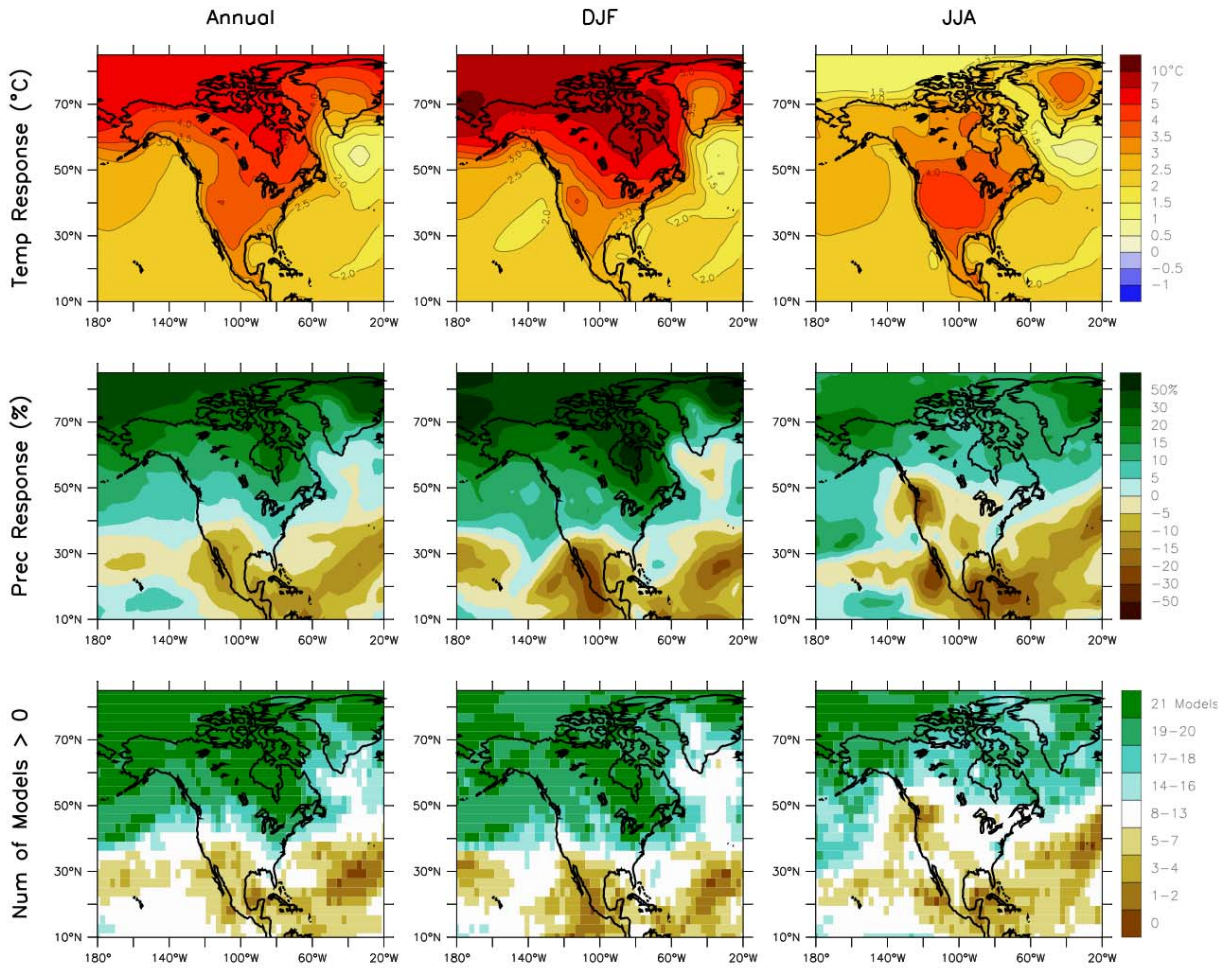

Figure 11.12. MMD-A1B temperature and precipitation changes over North America. Top row: Annual mean, December-January-February, and June-July-August temperature change between 1980–1999 and 2080–2099, averaged over 21 models. Middle row: same for fractional change in precipitation. Bottom row: number of models out of 21 that project precipitation to increase.

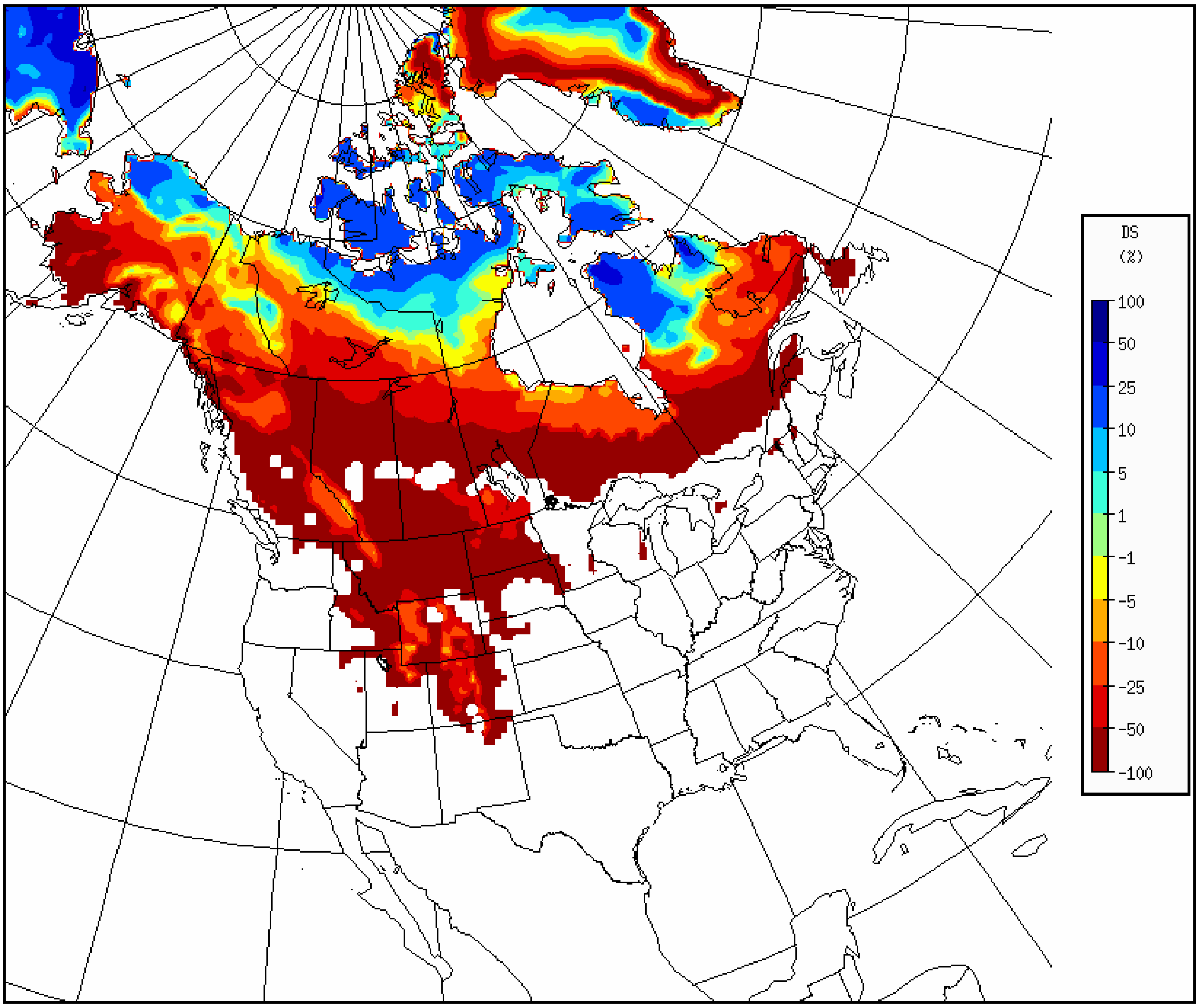

Figure 11.13. Percent snow depth changes in March (only calculated where climatological snow amounts exceed 5 mm of water equivalent), as projected by CRCM (Plummer et al., 2006), driven by CGCM, for 2041–2070 under SRES A2, using for reference 1961–1990.

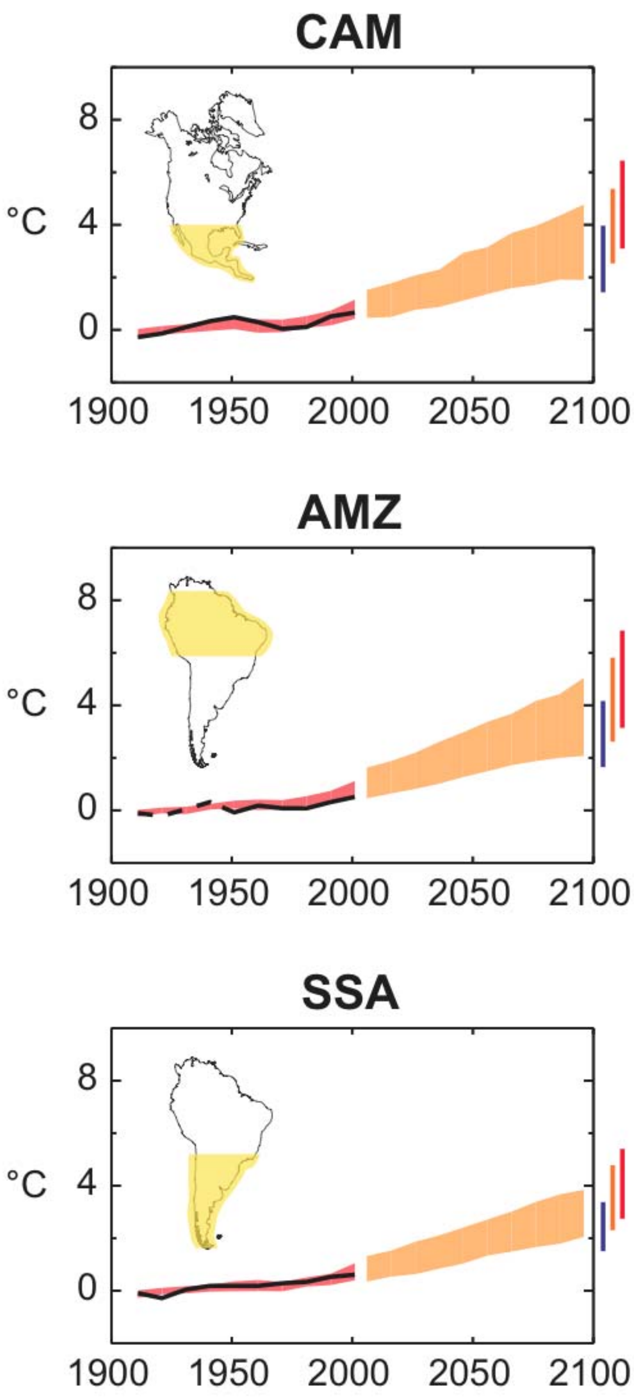

Figure 11.14. Temperature anomalies with respect to 1901–1950 for three Central and South American land regions for 1906–2005 (black line) and as simulated (red envelope) by MMD models incorporating known forcings; and as projected for 2001–2100 by MMD models for the A1B scenario (yellow envelope). The bars at the end of the yellow envelope represent the range of projected changes for 2091–2100 for the B1 scenario (blue), the A1B scenario (yellow) and the A2 scenario (red). The black line is dashed where observations are present for less than 50% of the area in the decade concerned. More details on the construction of these figures is given in Box 11.1 and Section 11.1.2

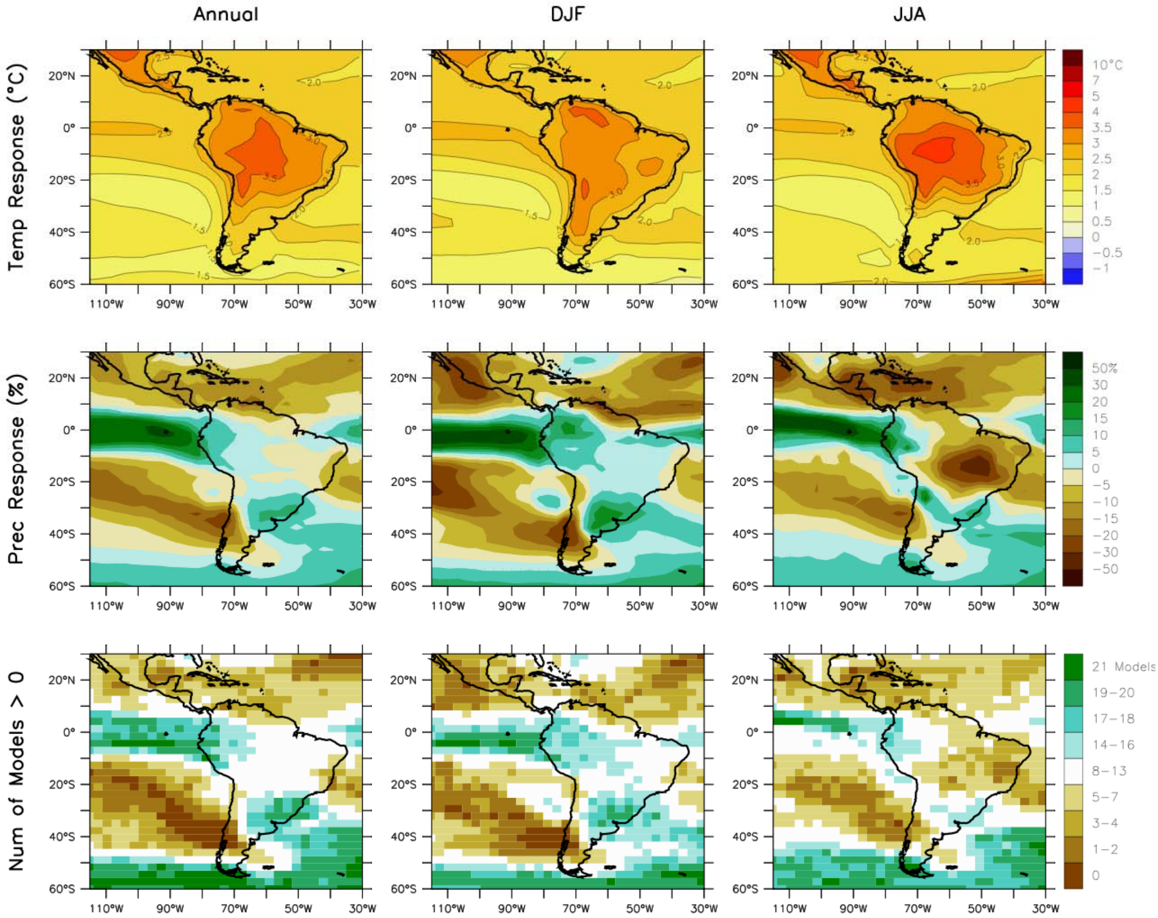

Figure 11.15. MMD-A1B temperature and precipitation changes over Central and South America. Top row: Annual mean, December-January-February, and June-July-August temperature change between 1980–1999 and 2080–2099, averaged over 21 models. Middle row: same for fractional change in precipitation. Bottom row: number of models out of 21 that project precipitation to increase.

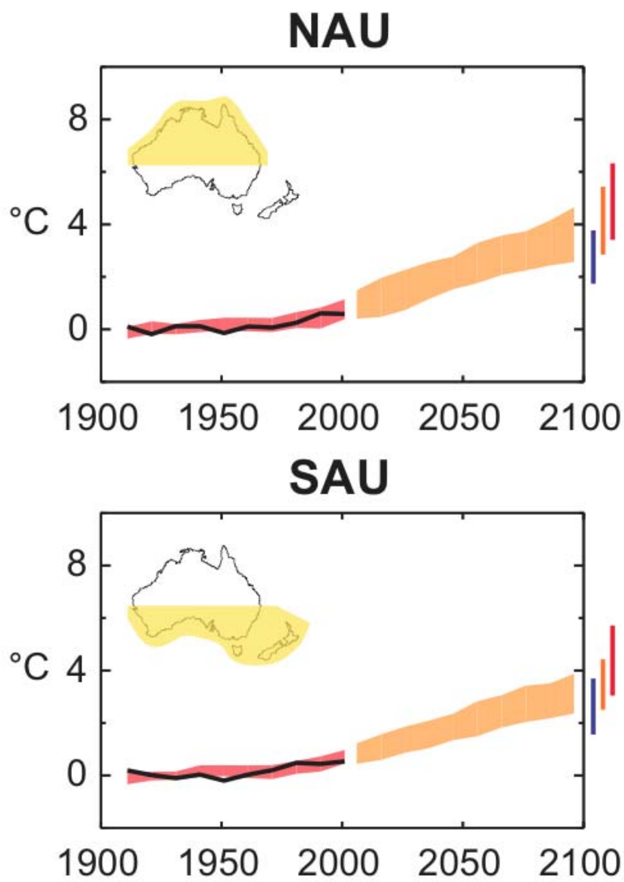

Figure 11.16. Temperature anomalies with respect to 1901–1950 for two Australian land regions for 1906–2005 (black line) and as simulated (red envelope) by MMD models incorporating known forcings; and as projected for 2001–2100 by MMD models for the A1B scenario (yellow envelope). The bars at the end of the yellow envelope represent the range of projected changes for 2091–2100 for the B1 scenario (blue), the A1B scenario (yellow) and the A2 scenario (red). The black line is dashed where observations are present for less than 50% of the area in the decade concerned. More details on the construction of these figures is given in Box 11.1 and Section 11.1.2.

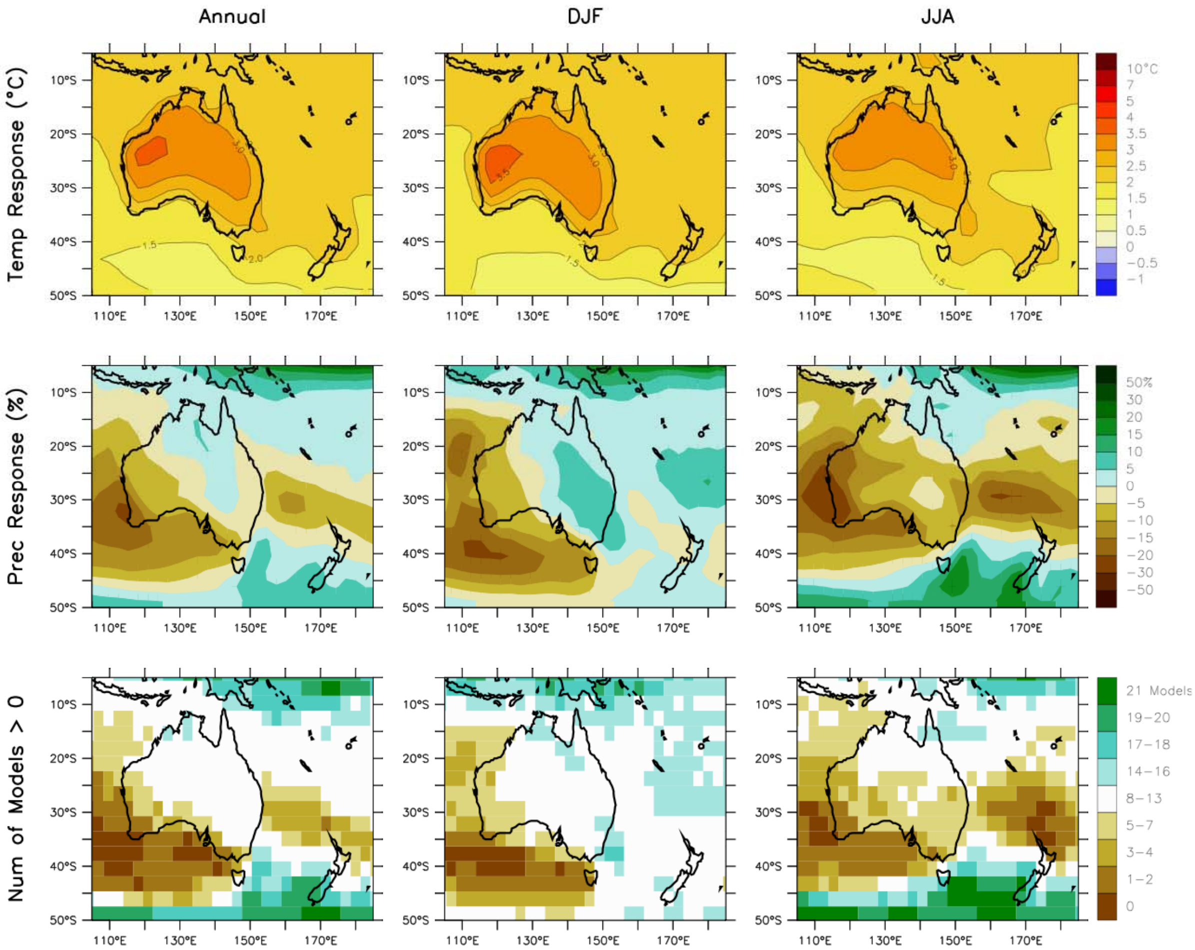

Figure 11.17. MMD-A1B temperature and precipitation changes over Australia and New Zealand. Top row: Annual mean, December-January-February, and June-July-August temperature change between 1980–1999 and 2080–2099, averaged over 21 models. Middle row: same for fractional change in precipitation. Bottom row: number of models out of 21 that project precipitation to increase.

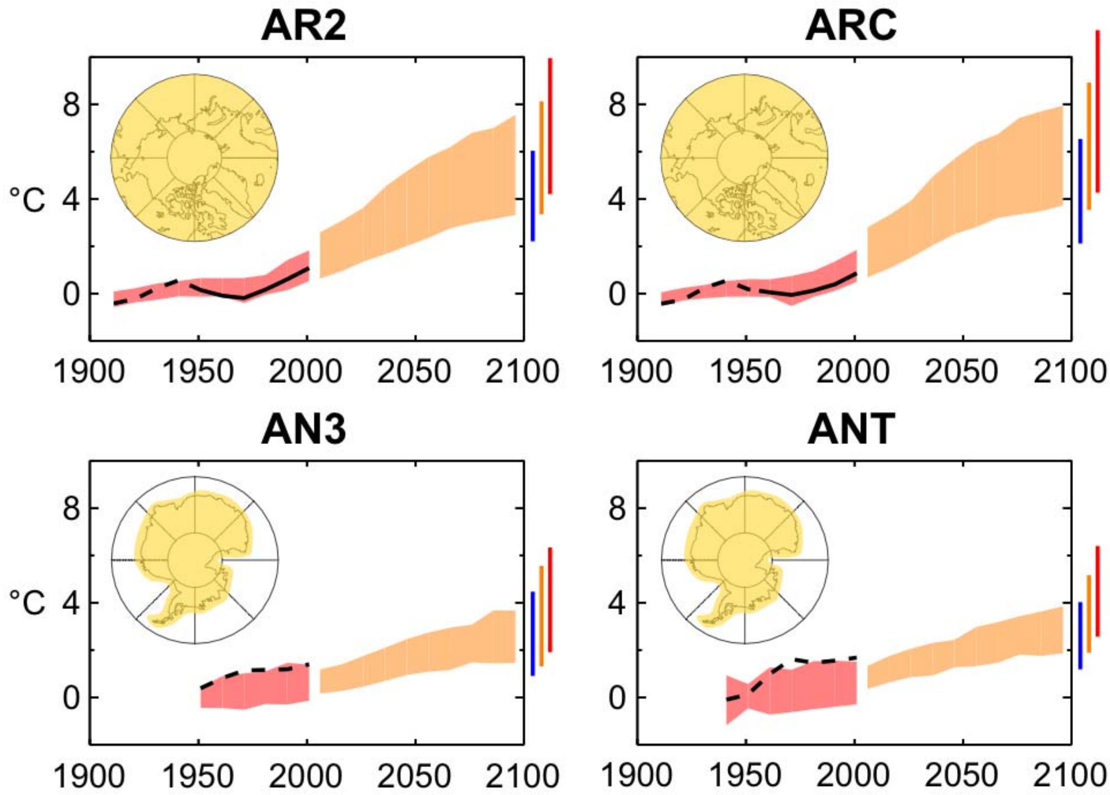

Figure 11.18. Left panel: Temperature anomalies with respect to 1901–1950 for the whole Arctic for 1906–2005 (black line) as simulated (red envelope) by MMD models incorporating known forcings; and as projected for 2001–2100 by MMD models for the A1B scenario (yellow envelope). The bars at the end of the yellow envelope represent the range of projected changes for 2091–2100 for the B1 scenario (blue), the A1B scenario (yellow) and the A2 scenario (red). The black line is dashed where observations are present for less than 50% of the area in the decade concerned. Right panel: The same for Antarctic land, but with observations for 1936–2005 and anomalies calculated with respect to 1951–2000. More details on the construction of these figures is given in Box 11.1 and Section 11.1.2

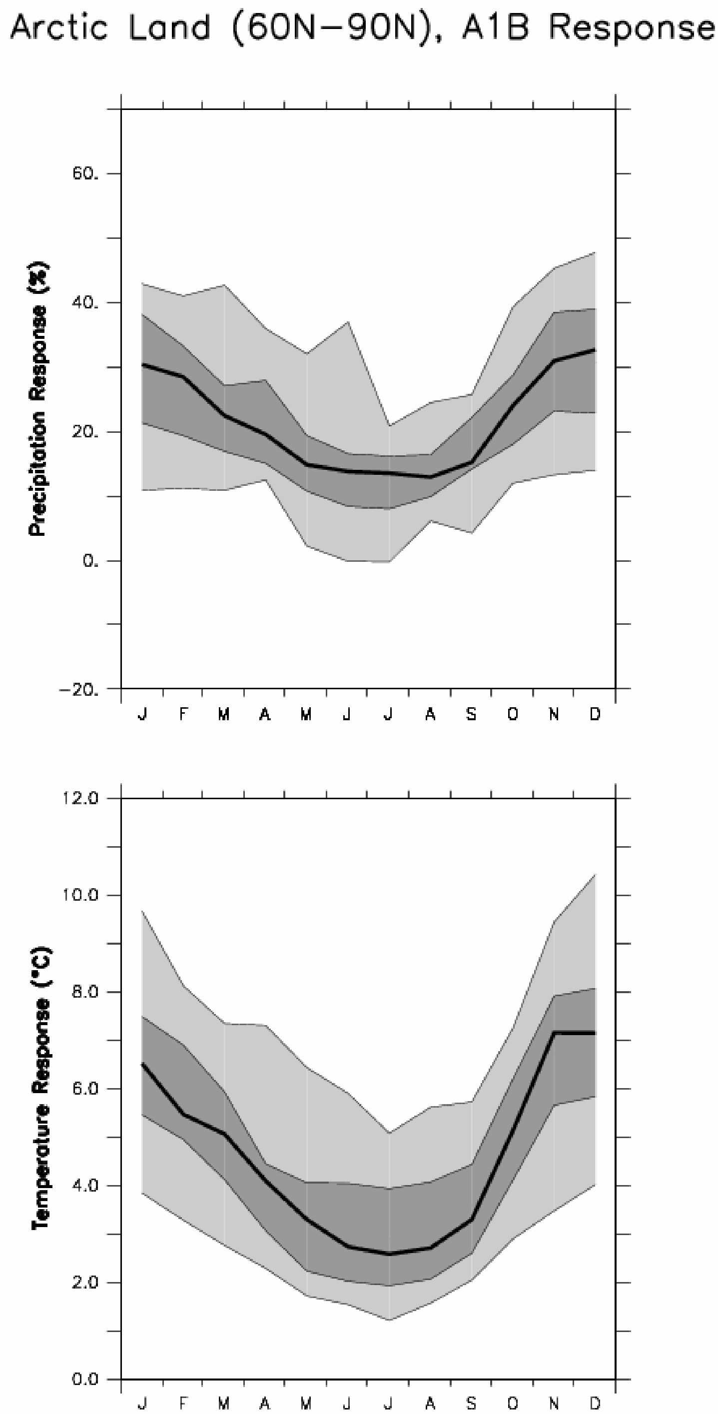

Figure 11.19. Annual cycle of Arctic area mean temperature and percentage precipitation changes (averaged over the area north of 60°N) for 2080–2099 minus 1980–1999, under the A1B scenario. Thick lines represent the ensemble median of the 21 MMD models. The dark grey area represents the 25% and 75% quartile values among the 21 models, while the light grey area shows the total range of the models.

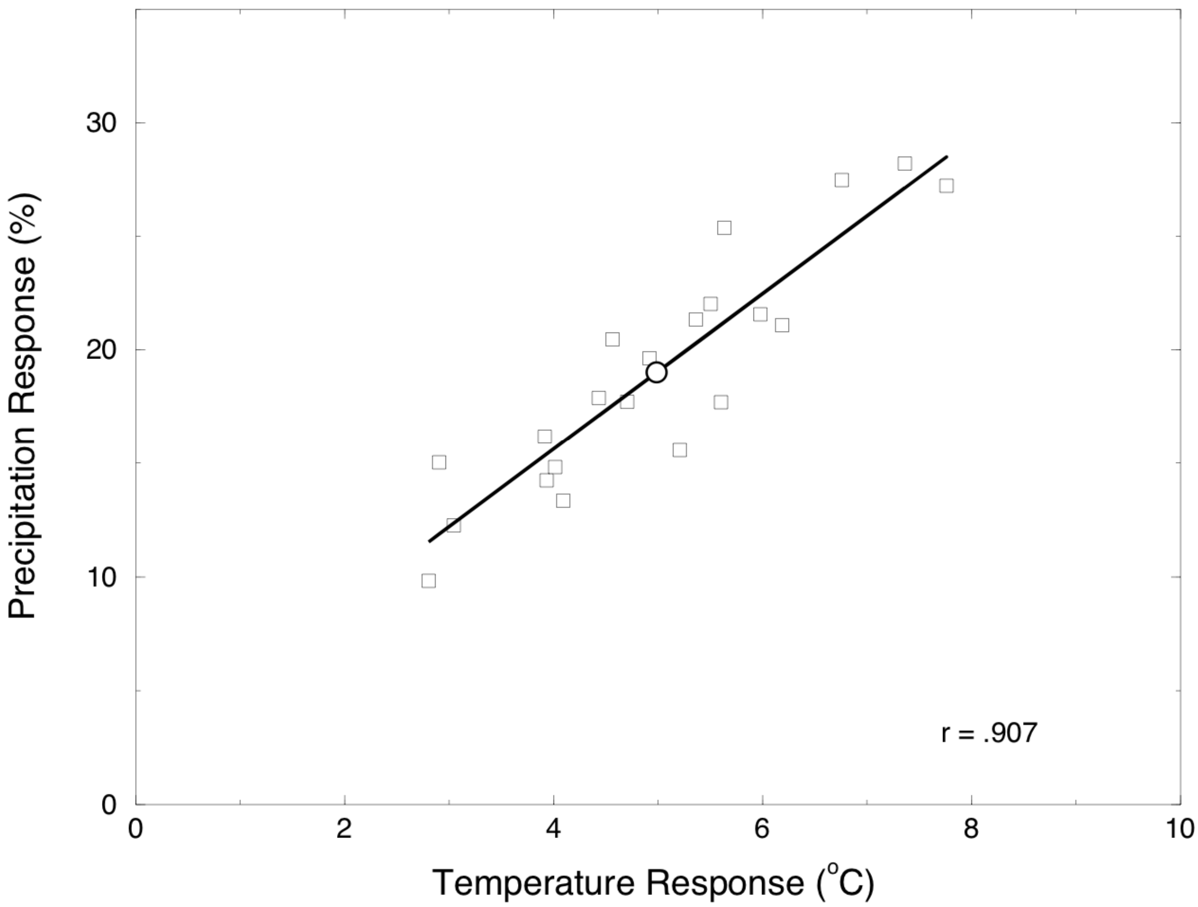

Figure 11.20. Relationship between the annual percentage precipitation and temperature change (2080–2099 minus 1980–1999) in the Arctic (averaged over the area north of 60°N) in the MMD-A1B projections. The model ensemble mean response is indicated by the circle.

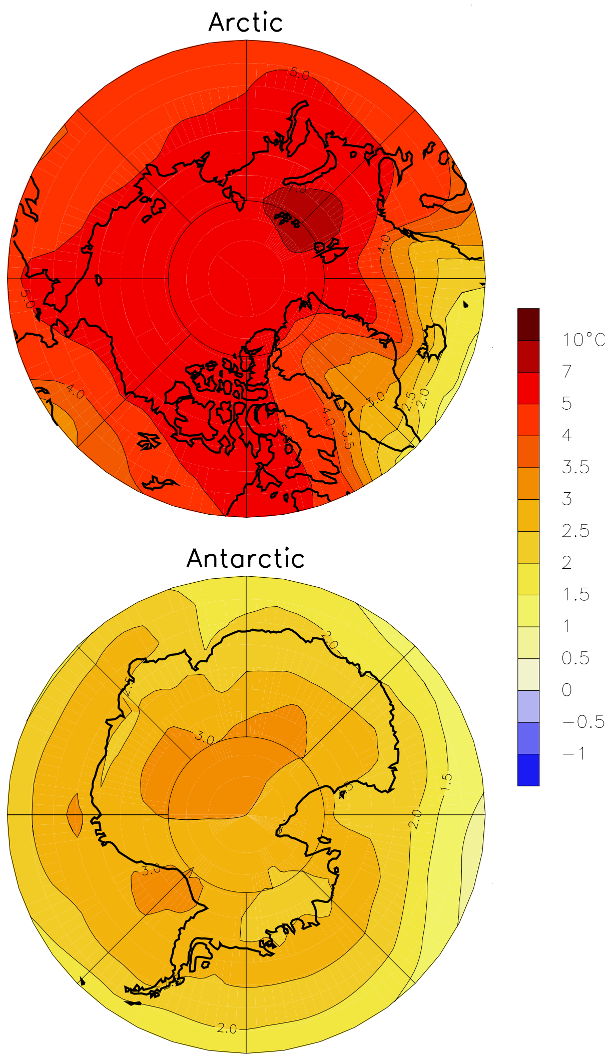

Figure 11.21. Annual surface temperature change from from 1980–1999 to 2080–2099 in the Arctic and Antarctic for the MMD-A1B projections.

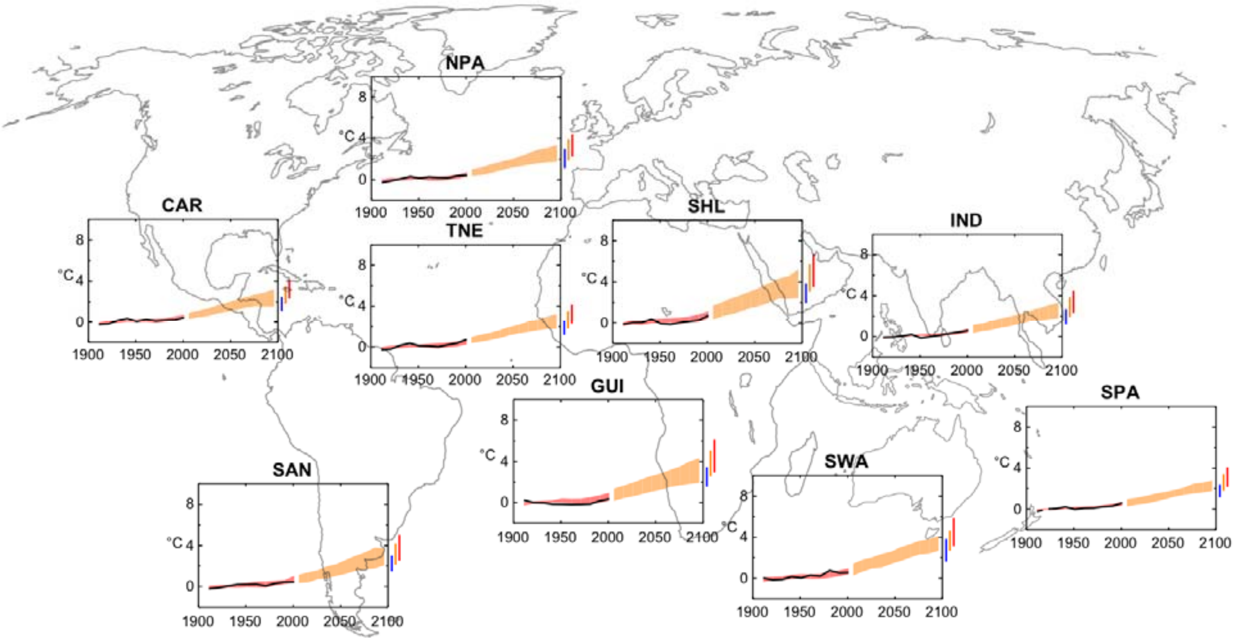

Figure 11.22. Temperature anomalies with respect to 1901–1950 for six Oceanic regions for 1906–2005 (black line) and as simulated (red envelope) by MMD models incorporating known forcings; and as projected for 2001–2100 by MMD models for the A1B scenario (yellow envelope). The bars at the end of the yellow envelope represent the range of projected changes for 2091–2100 for the B1 scenario (blue), the A1B scenario (yellow) and the A2 scenario (red). The black line is dashed where observations are present for less than 50% of the area in the decade concerned. More details on the construction of these figures is given in Box 11.1 and Section 11.1.2

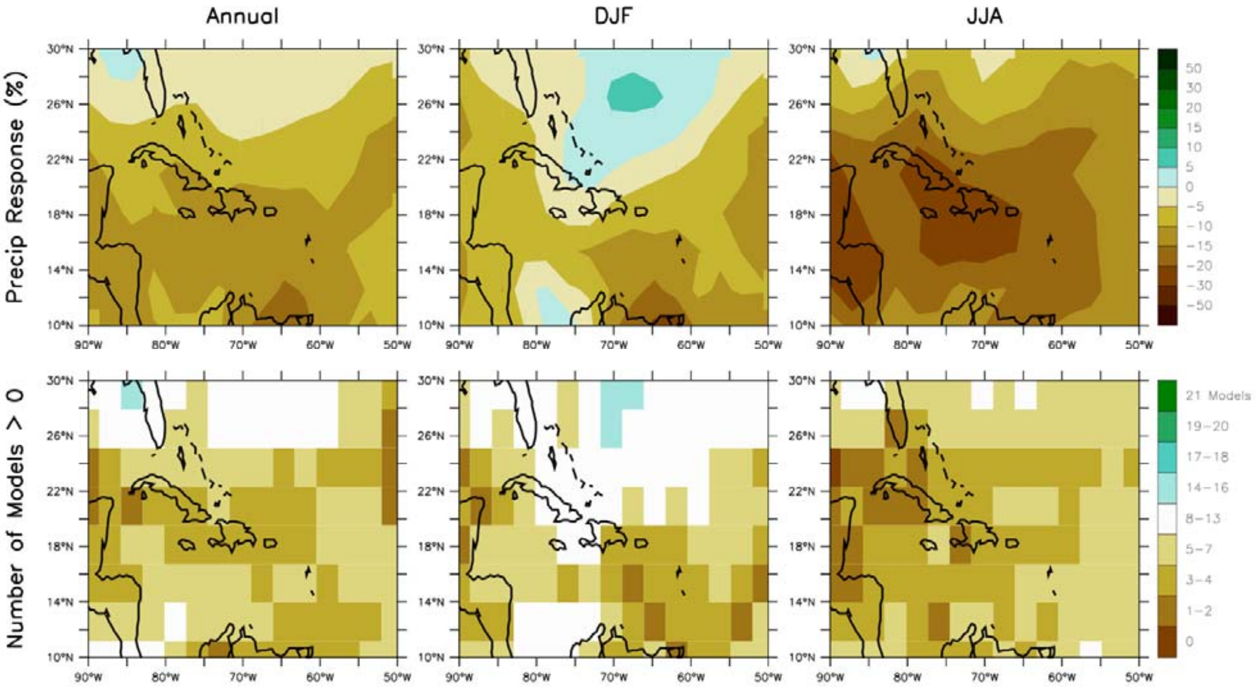

Figure 11.23. MMD-A1B temperature and precipitation changes over the Caribbean. Top row: Annual mean, December-January-February, and June-July-August temperature change between 1980–1999 and 2080–2099, averaged over 21 models. Middle row: same for fractional change in precipitation. Bottom row: number of models out of 21 that project precipitation to increase.

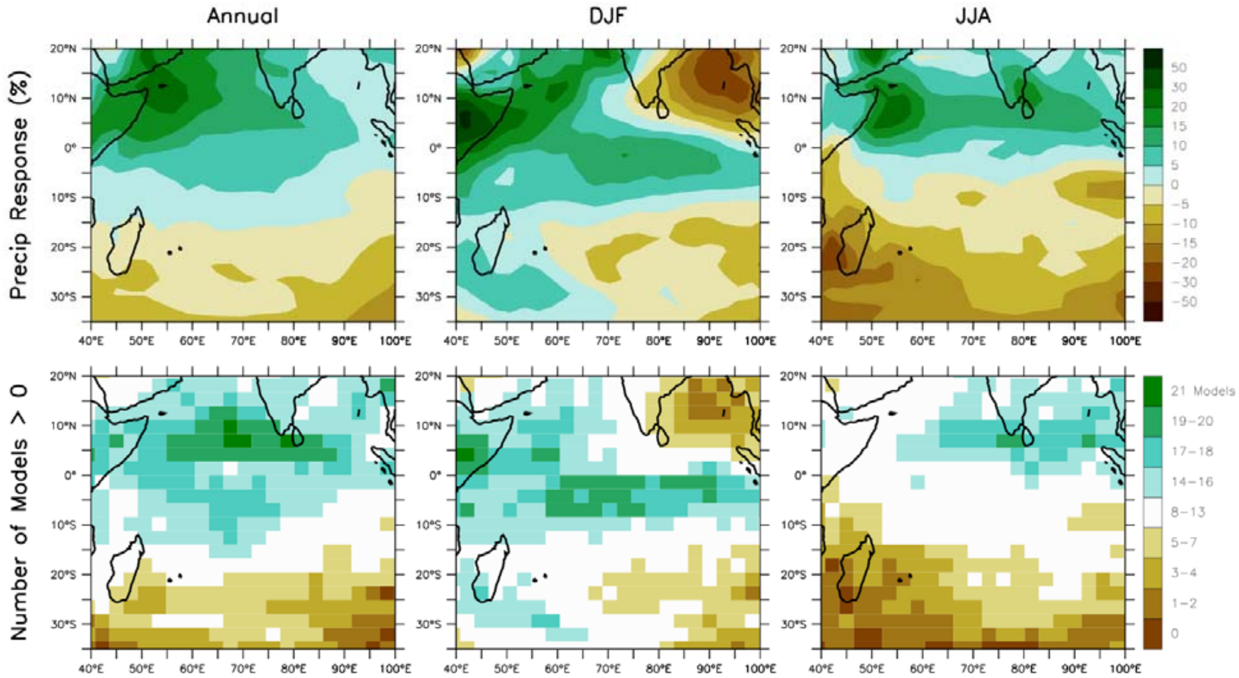

Figure 11.24. As for Figure 11.23 but for the Indian Ocean.

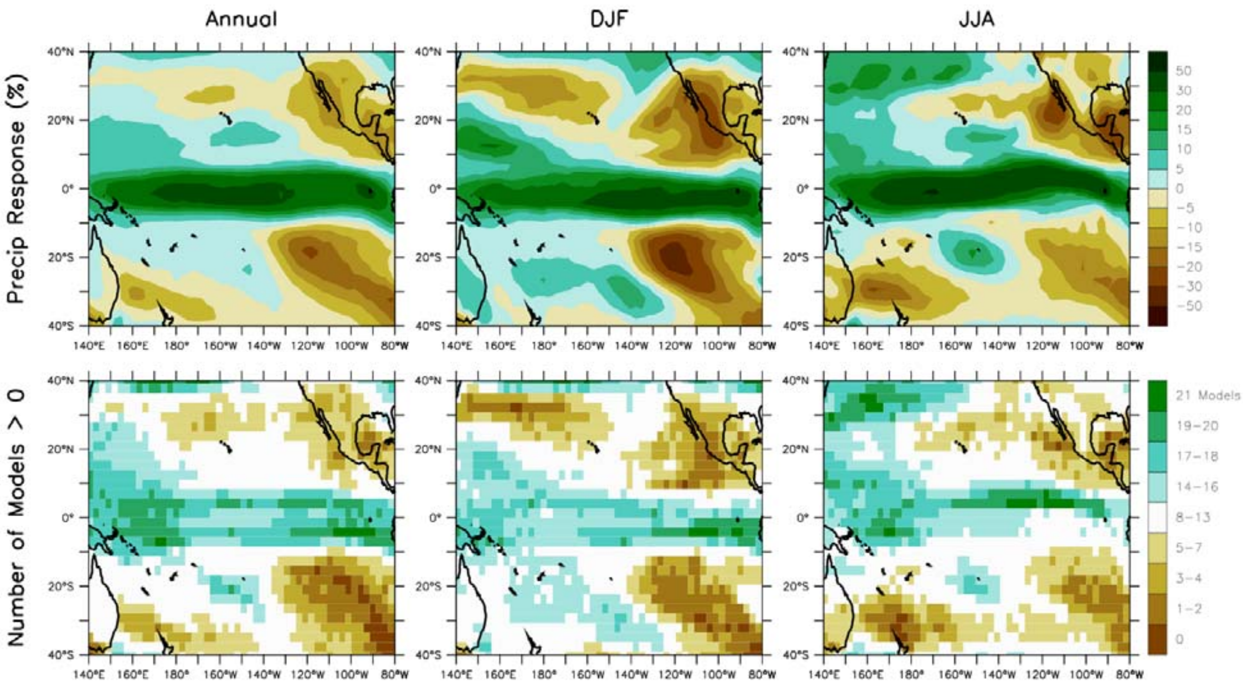

Figure 11.25. As for Figure 11.23 but for the northern and southern Pacific Ocean.

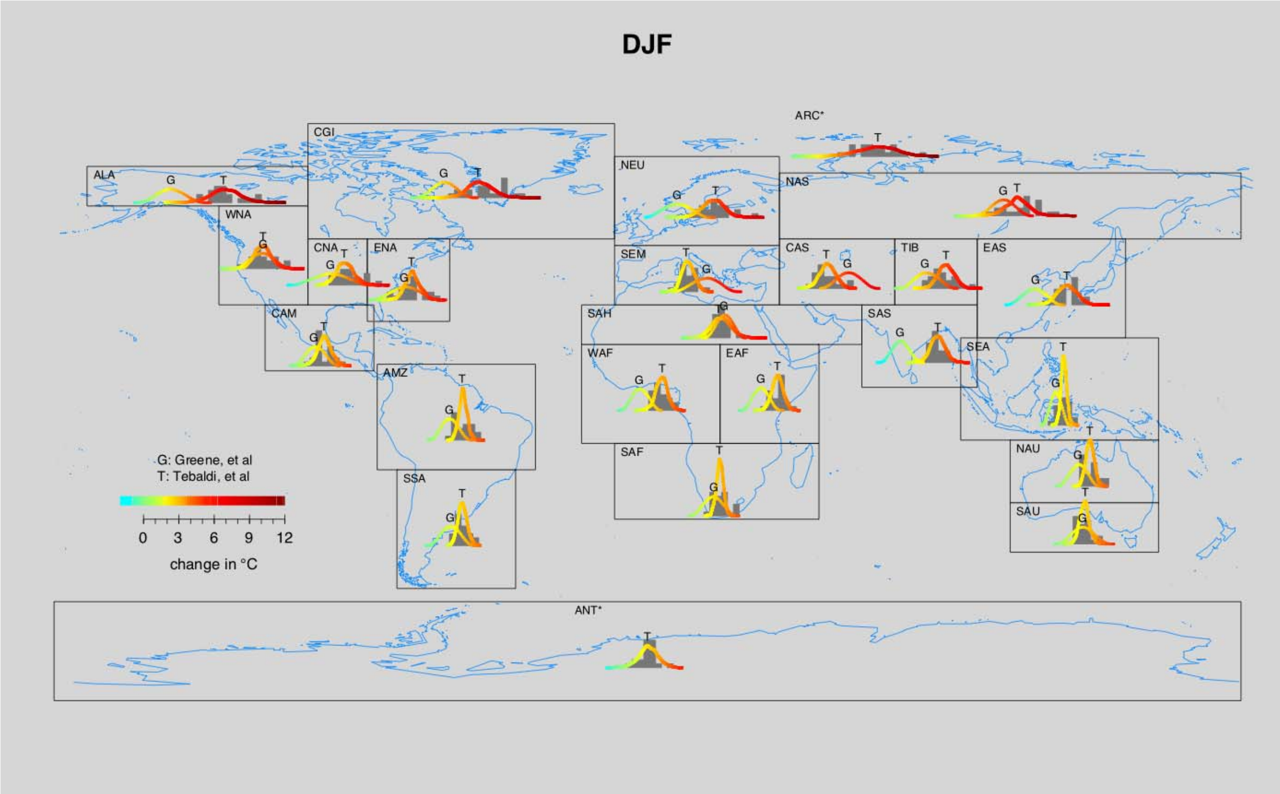

Figure 11.26. Map comparing probability density functions (PDFs) of change in temperature (2080–2099 vs. 1980–1999) for Tebaldi et al. (2004, 2005) and Greene et al. (2006) as well as the raw model projections (represented by shaded histograms) for the Giorgi and Francisco regions. Areas under the curves and areas covered by the histograms have been scaled to equal 1. The scenario is SRES A1B and the season is northern hemisphere winter (DJF). Asterisks adjacent to ARC and ANT regions indicate that only the Tebaldi et al. results were available.

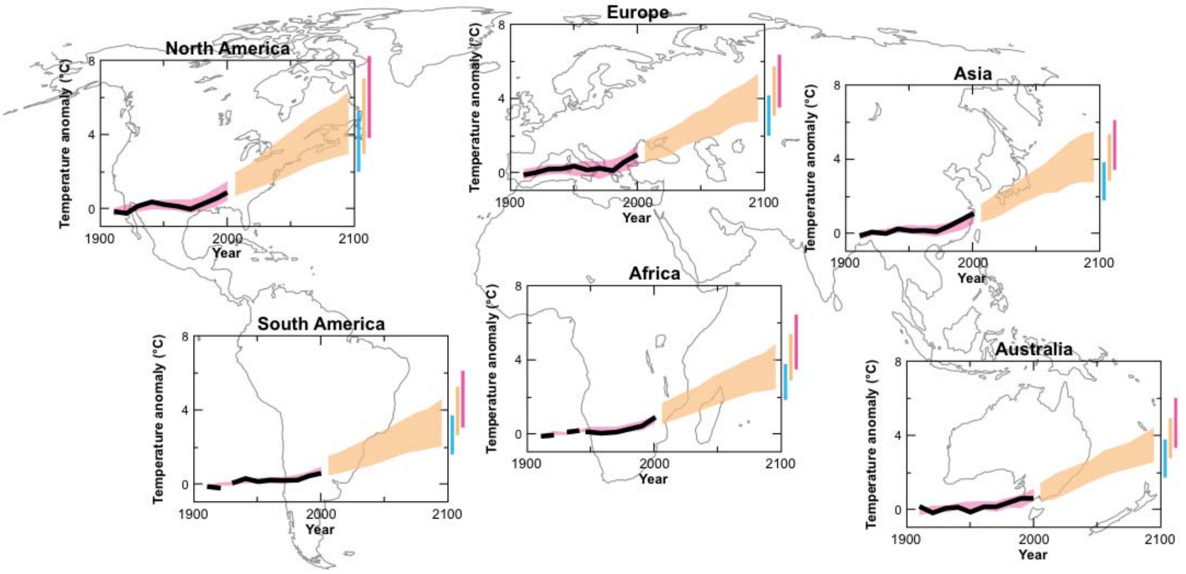

Box 11.1, Figure 1. Temperature anomalies with respect to 1901–1950 for six continental scale regions for 1906–2005 (black line) and as simulated (red envelope) by MMD models incorporating known forcings; and as projected for 2001–2100 by MMD models for the A1B scenario (yellow envelope). The bars at the end of the yellow envelope represent the range of projected changes for 2091–2100 for the B1 scenario (blue), the A1B scenario (yellow) and the A2 scenario (red). The black line is dashed where observations are present for less than 50% of the area in the decade concerned. More details on the construction of these figures is given in Box 11.1 and Section 11.1.2

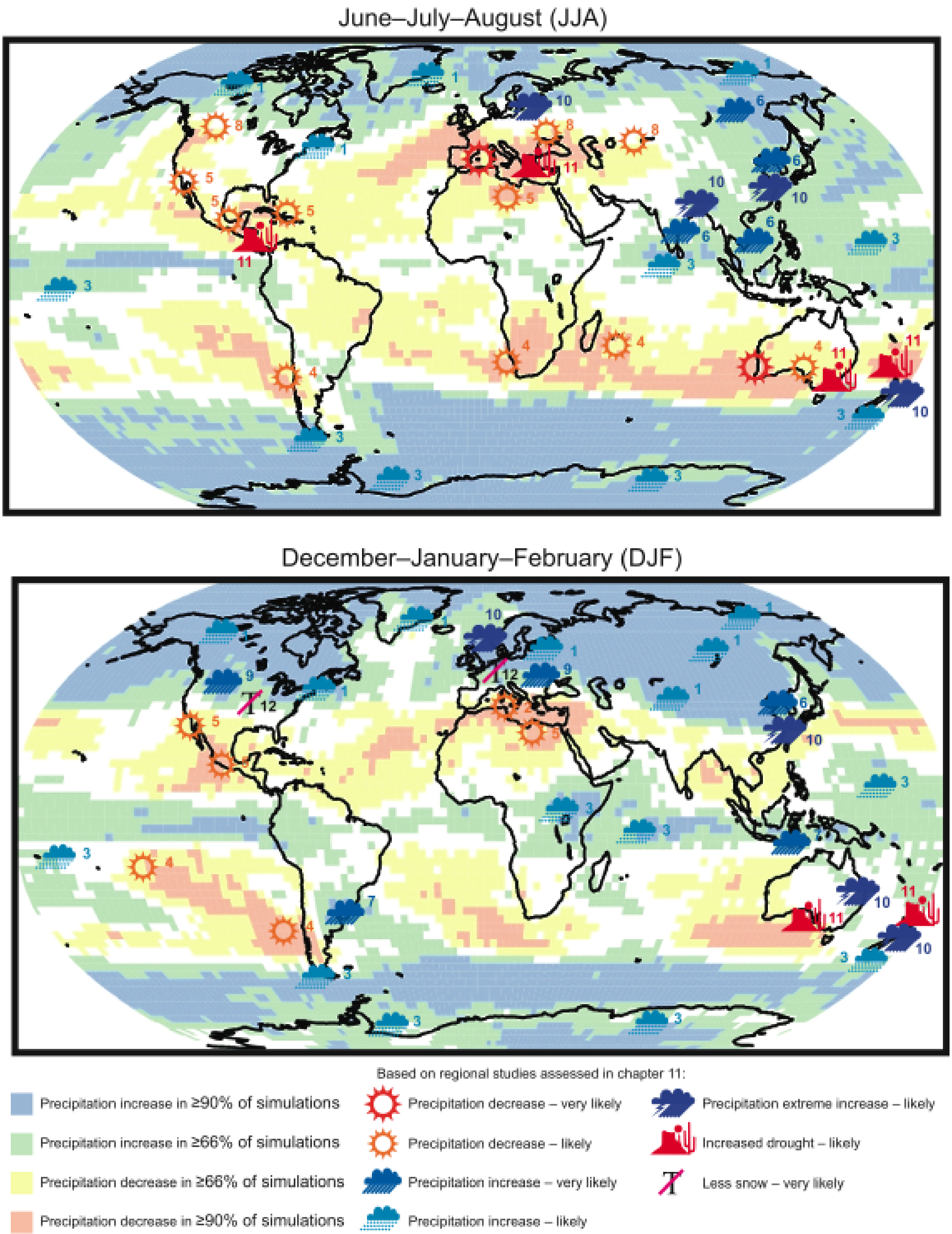

Box 11.1, Figure 2. Robust findings on regional climate change for mean and extreme precipitation, drought, snow, sea-ice, extreme winds and tropical cyclones. This regional assessment is based upon AOGCM based studies, RCMs, statistical downscaling and process understanding. More detail on these findings may be found in the notes below, and their full description, including sources is in Chapter 11. The background map indicates the degree of consistency between AR4 AOGCM simulations (21 simulations used) in the direction of simulated precipitation change.

(1) Very likely annual mean increase in most of northern Europe and the Arctic (largest in cold season), Canada, and the North-East USA; and winter (DJF) mean increase in Northern Asia and the Tibetan Plateau.
(2) Very likely annual mean decrease in most of the Mediterranean area, and winter (JJA) decrease in southwestern Australia.
(3) Likely annual mean increase in tropical and East Africa, Northern Pacific, the northern Indian Ocean, the South Pacific (slight, mainly equatorial regions), the west of the South Island of New Zealand, Antarctica and winter (JJA) increase in Tierra del Fuego.
(4) Likely annual mean decrease in and along the southern Andes, summer (DJF) decrease in eastern French Polynesia, winter (JJA) decrease for Southern Africa and in the vicinity of Mauritius, and winter and spring decrease in southern Australia.
(5) Likely annual mean decrease in North Africa, northern Sahara, Central America (and in the vicinity of the Greater Antilles in JJA) and in South-West USA.
(6) Likely summer (JJA) mean increase in Northern Asia, East Asia, South Asia and most of Southeast Asia, and likely winter (DJF) increase in East Asia.
(7) Likely summer (DJF) mean increase in southern Southeast Asia and southeastern South America
(8) Likely summer (JJA) mean decrease in Central Asia, Central Europe and Southern Canada.
(9) Likely winter (DJF) mean increase in central Europe, and southern Canada
(10) Likely increase in extremes of daily precipitation in northern Europe, South Asia, East Asia, Australia and New Zealand.
(11) Likely increase in risk of drought in Australia and eastern New Zealand; the Mediterranean, central Europe (summer drought); in Central America (boreal spring and dry periods of the annual cycle).
(12) Very likely decrease in snow season length and likely to very likely decrease in snow depth in most of Europe and North America.

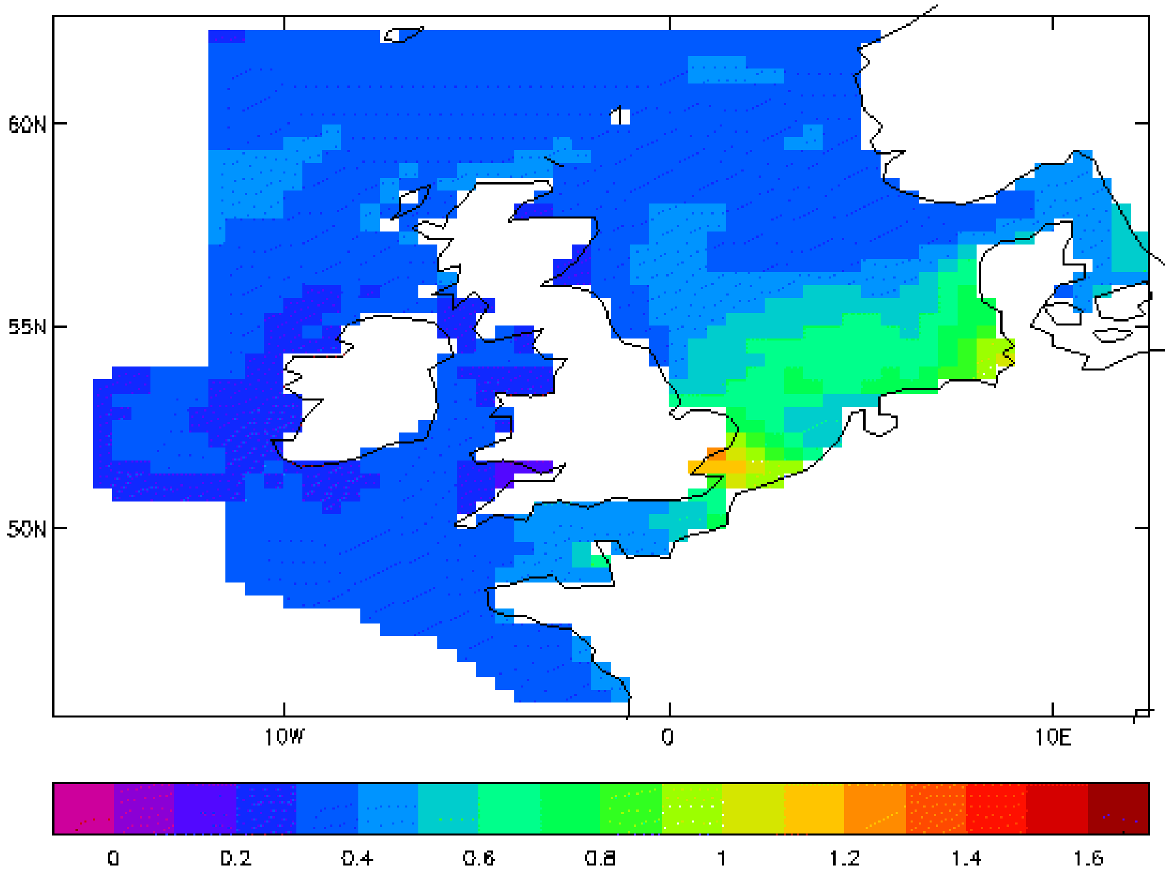

Box 11.4, Figure 1. Change in the 50-year return period extreme water level (in metres) in the North Sea due to changes in atmospheric storminess, mean sea level and vertical land movements for the period 2071–2100 under the A2 scenario (from Lowe and Gregory, 2005).

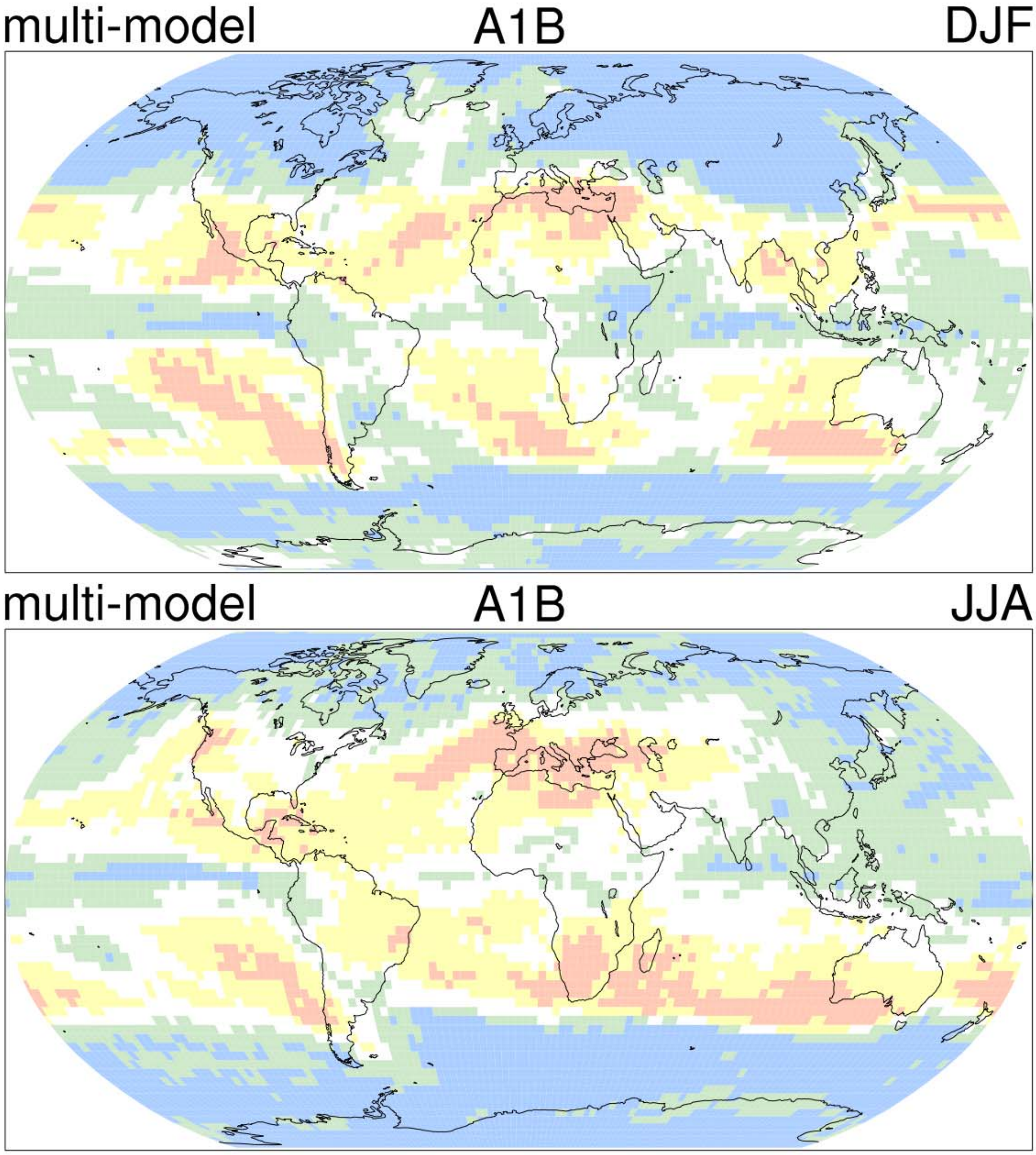

FAQ 11.1, Figure 1. Blue and green areas on the map are projected to experience increases in precipitation, while areas in yellow and pink are projected to have decreases.